

## Dynamic actuation of a novel laser-processed NiTi linear actuator

This article has been downloaded from IOPscience. Please scroll down to see the full text article.

2012 Smart Mater. Struct. 21 094004

(<http://iopscience.iop.org/0964-1726/21/9/094004>)

View [the table of contents for this issue](#), or go to the [journal homepage](#) for more

Download details:

IP Address: 129.97.27.27

The article was downloaded on 11/09/2012 at 23:50

Please note that [terms and conditions apply](#).

# Dynamic actuation of a novel laser-processed NiTi linear actuator

A Pequegnat<sup>1</sup>, M Daly<sup>1</sup>, J Wang<sup>1</sup>, Y Zhou<sup>1</sup> and M I Khan<sup>1,2</sup>

<sup>1</sup> Centre for Advanced Materials Joining (CAMJ), Department of Mechanical and Mechatronics Engineering, University of Waterloo, 200 University Avenue West, Waterloo, ON, N2L 3G1, Canada

<sup>2</sup> Smarter Alloys Incorporated, MaRS Centre, South Tower, 101 College Street, Suite 200, Toronto, ON, M5G1L7, Canada

E-mail: [apequegn@uwaterloo.ca](mailto:apequegn@uwaterloo.ca)

Received 5 January 2012, in final form 13 April 2012

Published 31 August 2012

Online at [stacks.iop.org/SMS/21/094004](http://stacks.iop.org/SMS/21/094004)

## Abstract

A novel laser processing technique, capable of locally modifying the shape memory effect, was applied to enhance the functionality of a NiTi linear actuator. By altering local transformation temperatures, an additional memory was imparted into a monolithic NiTi wire to enable dynamic actuation via controlled resistive heating. Characterizations of the actuator load, displacement and cyclic properties were conducted using a custom-built spring-biased test set-up. Monotonic tensile testing was also implemented to characterize the deformation behaviour of the martensite phase. Observed differences in the deformation behaviour of laser-processed material were found to affect the magnitude of the active strain. Furthermore, residual strain during cyclic actuation testing was found to stabilize after 150 cycles while the recoverable strain remained constant. This laser-processed actuator will allow for the realization of new applications and improved control methods for shape memory alloys.

## 1. Introduction

Shape memory alloy (SMA) materials are a prime candidate for actuation applications due to their unique functional thermomechanical characteristics, namely the shape memory effect (SME). A simple SMA actuator has the potential to replace complex electromechanical systems, allowing for reductions in cost, size and weight [1, 2]. However, until recently SMAs have only been able to exhibit a single SME, which has limited the functionality of monolithic components. As a result, complex control systems are required to activate traditional SMA actuators in a dynamic fashion [1–4]. In order to achieve dynamic actuation of traditional single memory SMA actuators, minor (or inner) hysteresis loops are often used [2]. Only partial transformation of the alloy occurs using this method, leading to partial activation. There are several drawbacks to this method for dynamic actuation which include: (i) minor hysteresis loops are not well understood and do not resemble the major loop, making precise control difficult [5]; (ii) feedback such as displacement, load, temperature or resistance is necessary and the relation to the degree of actuation is not straightforward [2, 3, 6–9]; and

(iii) the operating temperatures are narrow and bound by the transformation temperatures of the specific alloy.

The state-of-the-art processing technique, referred to as multiple memory material (MMM) technology, has demonstrated the ability to locally alter thermomechanical properties of conventional NiTi SMAs [10–15]. Using a high power density energy source (i.e. electron beam, arc, laser, etc) the local functional properties of a monolithic NiTi component can be augmented. These local modifications to thermomechanical properties have been attributed to microstructural and compositional changes that subsequently alter transformation temperatures [10–17]. Phase transformation onset temperatures of NiTi alloys have been shown to be extremely sensitive to processing history [18, 19]. Hence, the slightest modifications can make drastic changes that can be exploited to enhance component functionality.

The current work demonstrates increased functionality and improved controllability of a resistively actuated linear actuator that has been laser-processed. Part of a monolithic NiTi wire was processed, creating a two-memory linear actuator capable of two distinct actuations via resistive heating. This design will enable new applications to be realized while greatly improving existing SMA devices.

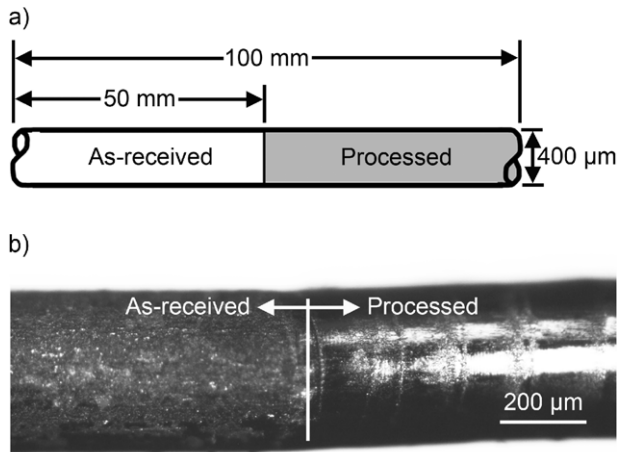


**Figure 1.** Schematic illustration of linear actuator (not to scale) (a) and optical micrograph of interface between as-received region and laser processed region (b).

## 2. Experimental details

### 2.1. Material

Commercially available 410  $\mu\text{m}$  (0.016 in) diameter Ni-49.2 at.% Ti wire, manufactured by Memry Corporation, was used in this study. This particular material was thermomechanically processed by the manufacturer to exhibit pseudoelasticity at room temperature. Prior to laser processing, the wire was chemically etched in a diluted solution of hydrofluoric and nitric acid to remove a thick black surface oxide, uniformly reducing the wire diameter to 400  $\mu\text{m}$ .

### 2.2. Laser processing

Laser processing was performed using a Miyachi Unitek LW50A pulsed Nd:YAG laser system with a spot size of 600  $\mu\text{m}$ . An argon shielding gas with a flow rate of 0.42  $\text{m}^3 \text{h}^{-1}$  (15 CFH) was found to be sufficient to avoid oxidation during processing. Laser processing parameters (i.e. peak power, pulse shape, frequency, etc) were altered to control the transformation temperatures during processing [10, 11]. In this study the parameters were selected in order to establish two distinct actuations of the linear actuator; one resulting from the SME of the as-received region and the second from the laser-processed region. Half of the 100 mm ( $\sim 4$  in) length of the linear actuator was processed as illustrated in figure 1(a). An optical micrograph of the interface between the as-received and processed regions is provided in figure 1(b).

### 2.3. Thermo-analytical analysis

A Thermal Analysis Q2000 differential scanning calorimeter (DSC) equipped with a refrigerated cooling system was used to identify the phase transformation temperatures of the as-received and laser-processed materials. A modified version of the ASTM F2004-05 standard test method for

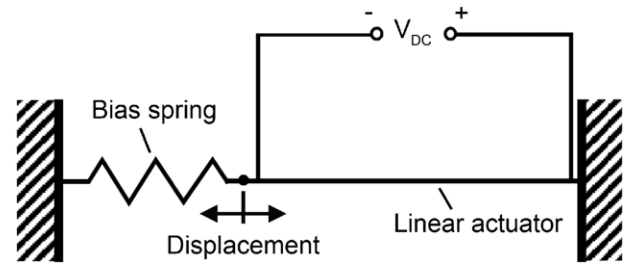


**Figure 2.** Illustration of the spring-biased linear actuator test set-up (not to scale).

the transformation temperature of NiTi alloys by thermal analysis was adhered to. Deviation from the standard includes the testing temperatures which ranged between  $-75$  and  $100^\circ\text{C}$ , controlled at a rate of  $5^\circ\text{C min}^{-1}$ . The start and finish transformation temperatures—*austenite start* ( $A_s$ ), *austenite finish* ( $A_f$ ), *martensite start* ( $M_s$ ) and *martensite finish* ( $M_f$ )—were determined as per the American Society for Testing and Materials standard.

### 2.4. Performance characterization

**2.4.1. Dynamic actuation.** A custom test set-up was constructed to characterize the performance of the laser-processed linear actuator. A spring-biased configuration was chosen, as illustrated in figure 2, similar to that used in [1, 2, 4, 12]. To ensure that the actuator was completely in the martensite phase prior to heating, dry ice was used; maintaining an actuator resting temperature below  $-50^\circ\text{C}$ . A pre-stress of 234 MPa (i.e. 3 kg-f load) was applied via the bias spring to achieve the required initial strain in the martensite phase to enable the SME. Actuation was achieved by resistive heating causing the NiTi material to change phases from martensite to austenite and subsequently actuate by recovering the initial strain induced by the bias spring. A constant voltage Sorensen XG 33-25 programmable direct current (DC) power supply was used to supply the required power. The displacement, load and electrical resistance were measured during testing using a National Instruments PXI-1031 data acquisition (DAQ) module. The change in actuator length (i.e. displacement) was measured using a  $\pm 0.2 \mu\text{m}$  sensitivity Heidenhain displacement sensor and the load was measured using a 500 N load cell.

**2.4.2. Tensile testing.** Deformation of the as-received and laser-processed materials was assessed using a temperature-chamber-equipped Instron model 5548 micro-tensile tester with a  $\pm 0.5 \mu\text{m}$  measurement accuracy. Test samples having a 30 mm length were loaded at temperatures below  $M_f$  of the as-received and laser-processed materials under an ASTM F2516-07 testing protocol at a rate of  $0.8 \text{ mm min}^{-1}$ . The tests performed at  $-50^\circ\text{C}$  were designed to mimic the conditions during initial straining of the actuator prior to actuation while the tests performed at  $30^\circ\text{C}$  were representative of the condition of the laser-processed region of the actuator following actuation of the as-received region.

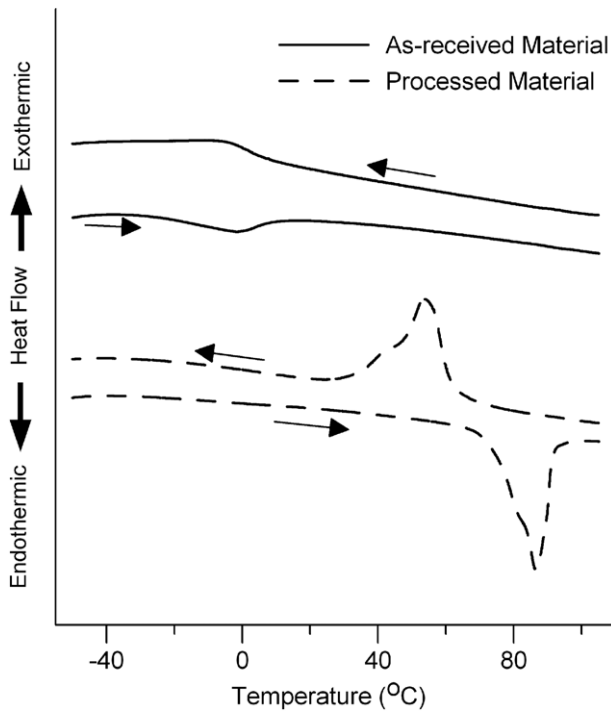


Figure 3. DSC data for as-received and laser-processed materials.

**2.4.3. Low cycle testing.** Low cycle actuation testing of the linear actuator was performed in the temperature chamber of the Instron micro-tensile tester at a constant temperature of  $-50^{\circ}\text{C}$ . The actuator was activated through 200 cycles consisting of a 10 s resistive heating segment where the temperature of the actuator wire reached above  $A_f$  of both the as-received and laser-processed materials followed by a 10 s cooling segment where the actuator was allowed to cool below the  $M_f$  of both materials. A constant load of 234 MPa (i.e. 3 kg-f load) was held by the cross-head while displacement was measured versus time. A 50 mm actuator was used in cyclic testing due to a size limitation of the temperature chamber. The recoverable ( $\varepsilon_r$ ) and residual ( $\varepsilon_p$ ) strains were extracted after each activation cycle.

### 3. Results and discussion

#### 3.1. Transformation temperatures

Thermal-analytical DSC results for both as-received and laser-processed materials are shown in figure 3. The  $A_s$ ,  $A_f$ ,  $M_s$  and  $M_f$  phase transformation temperatures extrapolated from the DSC curves are summarized in table 1. Transformation temperatures of the processed material increased significantly compared to the as-received material. Similar increases in transformation temperatures have been reported by Khan and Zhou [16], Tam *et al* [20] and Daly *et al* [14] following laser processing. In this study the  $A_f$  and  $M_f$  temperatures were increased by  $71.7^{\circ}\text{C}$  and  $46.6^{\circ}\text{C}$ , respectively. Hence, it was to be expected that during resistive heating less heat input (i.e. lower voltages) would be required to actuate the as-received region of the actuator compared to the

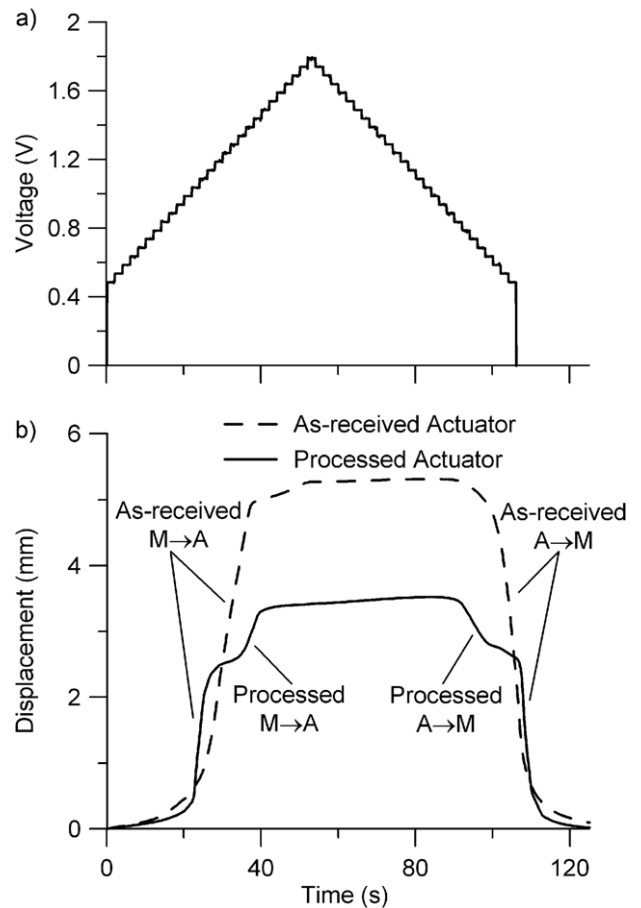


Figure 4. Voltage profile (a) and displacement measurements (b).

Table 1. Phase transformation temperatures ( $^{\circ}\text{C}$ ) from thermo-analytical DSC analysis.

	$A_s$	$A_f$	$M_s$	$M_f$
As-received material	-22.3	19.5	9.8	-14.6
Processed material	73.5	91.2	62.0	32.0

laser-processed region. For example, once the  $A_f$  temperature of the as-received region ( $19.5^{\circ}\text{C}$ ) has been reached, 50% of the wire will be in the austenite phase. Following further heating past the  $A_f$  temperature of the laser-processed region ( $91.2^{\circ}\text{C}$ ), the whole wire actuator will be in the austenite phase.

#### 3.2. Actuation

Actuation was induced using a voltage profile which first increased from 0.5 to 1.8 V then decreased back to 0.5 V while monitoring wire displacement. Voltage stepping of 0.05 V every 2 s was used to ensure steady heating and cooling, as shown in figure 4(a). With increasing voltage, wire temperature surpassed  $A_f$  for the as-received and laser-processed regions of the processed actuator; subsequently a decrease in voltage induced cooling below  $M_f$  of both regions. Figure 4(b) shows the two distinct actuations

in the displacement measurement for the laser-processed actuator. Upon application of voltage, first the as-received region transformed from martensite to austenite causing the processed actuator to initially recover 2.48 mm of strain. Increasing the voltage further triggered the second actuation and recovery of an additional 1.0 mm of strain from the laser-processed region. As the voltage decreased the reverse effect was observed: first the processed region transformed from austenite to martensite followed by the same transformation in the as-received region. The bias spring facilitates straining the actuator first by 1.0 mm then by 2.48 mm as the phase transformation to martensite takes place in the laser-processed and as-received regions, respectively. Also shown in figure 4(b) is the displacement trend from a 100 mm as-received actuator that was subject to the same voltage profile. Only one actuation was observed; however, 5.32 mm maximum displacement was achieved, a 34.6% larger active strain than the laser-processed actuator.

Through laser processing, different regions of the actuator were ‘programmed’ to fully actuate giving the desired load and displacement at specific temperatures. The length (i.e. volume) of each of the processed regions as well as the transformation temperature can be easily adjusted to obtain the desired response. Therefore, the need for partial transformation using minor hysteresis loops was not necessary for dynamic actuation. For example, a simple DC voltage profile such as that shown in figure 5(a) was used with the two-memory actuator developed in this study. In the first voltage pulse the voltage was increased to 1.4 V allowing for quick heating of the linear actuator and subsequently actuation of the as-received region. The voltage was then backed off slightly to 1.1 V maintaining a temperature just above the  $A_f$  of the as-received region. Following the first actuation a displacement of 2.48 mm was achieved yielding a 274 MPa stress. Next the voltage was increased to 1.8 V, increasing the temperature above the  $A_f$  of the laser-processed region, where the second actuation occurred. A total displacement of 3.48 mm was achieved, yielding a fully actuated stress of 287 MPa. Two distinct changes in resistance were also clearly observed in the resistance measurement shown in figure 5(c). This change in resistance has proven to be useful when developing control systems for SMA actuators [2, 3].

As demonstrated, using a laser-processed actuator, greater control over the amount of actuation and the temperatures at which these actuations occur can be achieved using simple control methods. Also, laser-processed actuators can now be actuated in a passive manner where the temperature of the ambient environment gives the desired dynamic response, enabling countless new applications for SMAs.

### 3.3. Stress–strain behaviour

To better understand the performance of the laser-processed actuator, monotonic tensile tests were performed. The results from tests performed at  $-50^\circ\text{C}$ , simulating the initial pre-straining of the processed actuator, are presented in figure 6(a). The deformation behaviours of the martensite

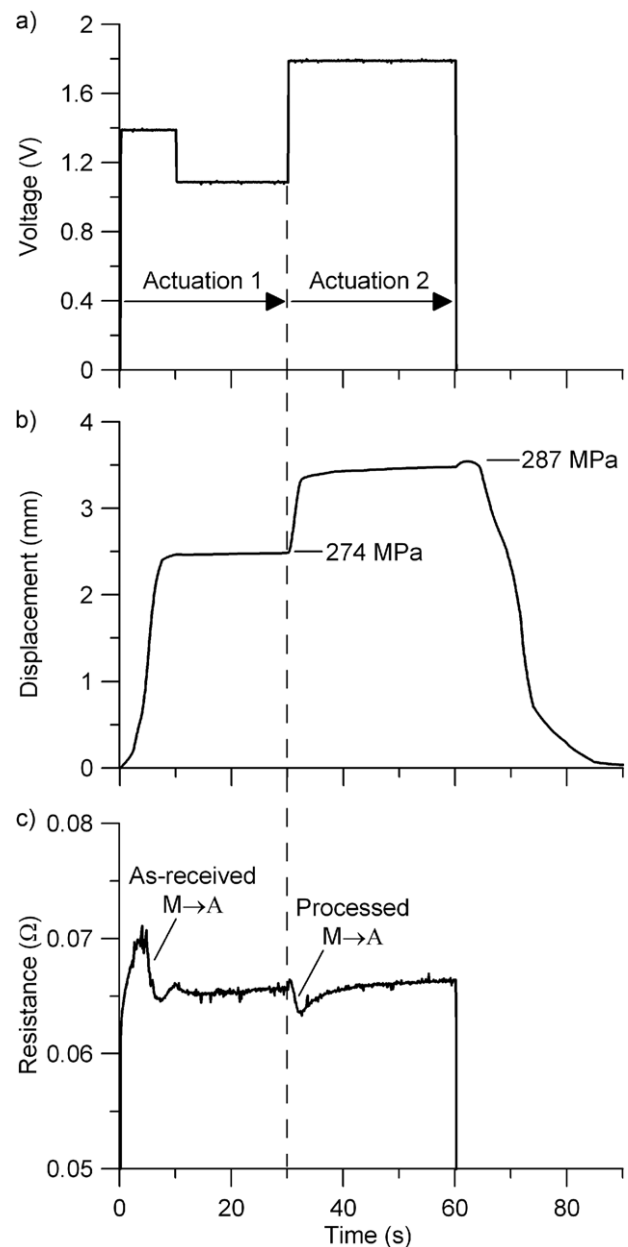


**Figure 5.** Dynamic actuation of a two-memory laser-processed linear actuator by resistive heating.

phase of as-received material and laser-processed material are shown for up to 10% strain. There are two notable differences in the stress–strain behaviour of the laser-processed material compared to the as-received material. These differences include the absence of the serrated, flat ‘Lüders-like deformation’ and a substantially larger martensite reorientation or flow stress ( $\sigma_M$ ) in the laser-processed material.

The presence of Lüders-like deformation in NiTi alloys is the result of the sudden reorientation of martensite during deformation resulting in the propagation of a macroscopic strain band [21]. This reorientation of martensite consists of neighbouring martensite variants becoming twin related, propagation/migration of the interface between neighbouring variants, and further detwinning of the reoriented martensite

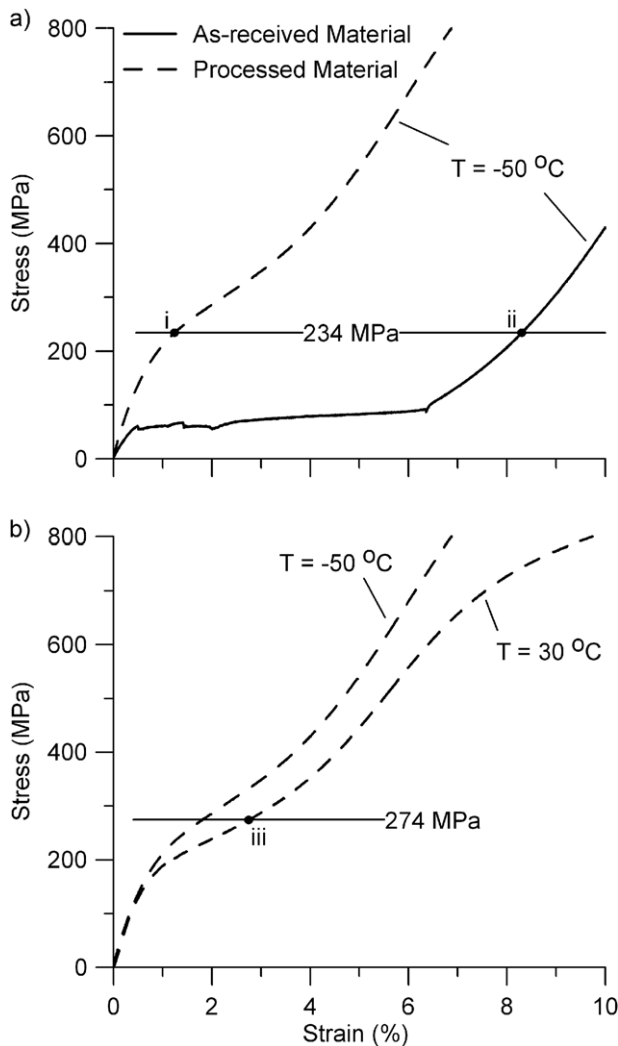


**Figure 6.** Detwinning of martensite in as-received and laser-processed regions at  $-50^{\circ}\text{C}$  (a) and comparison of detwinning stresses and strains at  $-50$  and  $30^{\circ}\text{C}$  for laser-processed material (b).

variants [22]. Once the stress exceeds the barrier stress for martensite reorientation the stress drops slightly and remains almost constant, creating the stress plateau as observed in the stress–strain curve for the as-received material in figure 6(a) [22, 23]. The ability of a strain band to propagate and lead to a stress plateau is heavily dependent on the texture of the NiTi alloy [21, 22, 24]. After initiation of the strain band no additional stress is necessary for propagation if a majority of the twinned martensite variants have a habit plane in the same direction as the local strain band [21]. The local stress concentration adjacent to the strain band is therefore sufficient to cause propagation. Liu *et al* [24] found when deforming martensite in the rolling direction that a stress plateau was possible. Murasawa *et al* [21] showed similar results with a rolled NiTi sheet that had been heat-treated below  $400^{\circ}\text{C}$ , where it was identified that the strain band and habit plane both exist at  $-55^{\circ}$  and  $+55^{\circ}$  to the loading direction. Therefore, it was deduced that during loading parallel to the drawing direction of the as-received wire

the texture of the material was such that the formation and propagation of a strain band was possible, leading to the stress plateau observed during the deformation of the martensite structure (figure 6(a)).

The absence of the Lüders-like deformation in the laser-processed material was also attributed to texture effects. Since the laser-processed material had solidification-type microstructure the texture was expected to be significantly different from the as-received drawn wire. The sloped strain-hardening behaviour observed in figure 6(a) for the laser-processed material was a result of the inability to form and propagate a macroscopic strain band. When the priority habit planes exist at several different angles relative to the loading direction, a single flow stress for martensite reorientation does not exist and therefore the sudden appearance of a stress plateau is not observed [21]. Increasing stresses are necessary to reorient martensite variants having different angles from the loading direction leading to the strain-hardening effect as observed for the laser-processed material in figure 6(a). Murasawa *et al* [21] and Liu *et al* [24] obtained similar strain-hardening trends during the tensile testing of NiTi sheets having a recrystallized texture and when loading in the transverse direction to the rolling direction, respectively. In planned future work the effects of laser processing on the texture will be studied in detail.

The greater  $\sigma_M$  of the laser-processed material shown in figure 6(a) was a result of the martensite in the laser-processed material being more stable at  $-50^{\circ}\text{C}$  than that in the as-received material. Since the reorientation of martensite is dependent on the movement of mobile defects, such as interfaces between neighbouring variants and twins which occur by thermal activation mechanisms, higher stress is required to cause reorientation. Miyazaki *et al* [25] showed that the flow stress increases with decreasing temperature below  $M_f$ . Since the difference between the test temperature of  $-50^{\circ}\text{C}$  and  $M_f$  of the laser-processed material was  $46.6^{\circ}\text{C}$  (or 57%) greater than that of the as-received material, a larger  $\sigma_M$  was expected.

#### 3.4. Effect of martensite properties on actuator performance

The strain-hardening behaviour of the laser-processed material and higher  $\sigma_M$  had a large effect on the active strain in the as-received and processed regions of the actuator. As denoted by (i) and (ii) in figure 6(a), the amount of initial strain in the processed and as-received regions following the 234 MPa pre-stress were 1.2% and 8.3%, respectively. The amount of strain experienced during the deformation of martensite is directly related to the magnitude of active strain possible via the SME [26]. Therefore, a greater displacement was expected during actuation of the as-received region of the actuator as observed in figures 4(b) and 5(b). From the activation of the as-received region 71.3% of the actuator's active strain was recovered. Following actuation of the as-received region the temperature of the actuator was above  $19.5^{\circ}\text{C}$ , the  $A_f$  temperature of the as-received material, and the stress reached 274 MPa. Therefore, the properties of

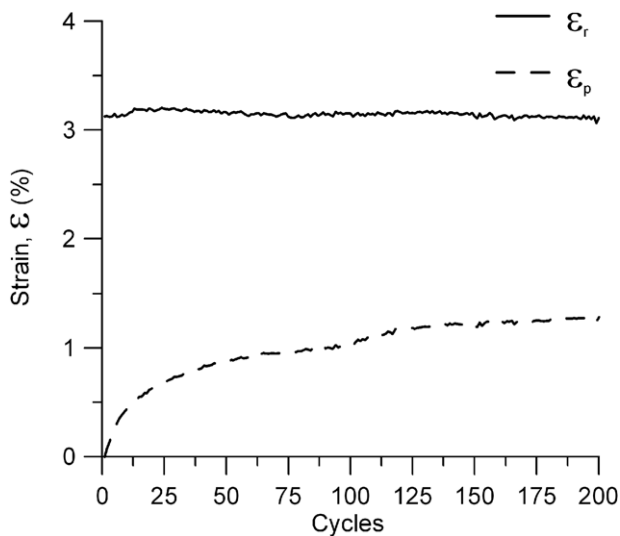


**Figure 7.** Recoverable strain ( $\varepsilon_r$ ) and residual strain ( $\varepsilon_p$ ) measured during cyclic actuation testing.

the laser-processed region must be considered under these conditions. Tensile tests performed at 30 °C for the processed material are therefore more representative at this stage of actuation. Since the stress has increased in the actuator following the first actuation and  $\sigma_M$  has decreased due to temperature effects, the strain in the laser-processed region has increased to 2.8% as indicated by (iii) in figure 6(b). The initial 2.8% strain in the laser-processed region was 25% of the total initial pre-straining in the actuator, corresponding well with the 28.9% recovery of active strain following the actuation of the laser-processed region (figures 4(b) and 5(b)). Hence, the interactions between the two different regions of the processed actuator having different thermomechanical properties becomes apparent and the smaller active strain compared to the as-received actuator (figure 4(b)) was explained.

### 3.5. Cyclic actuation performance

During the processing of SMAs for actuation applications it is critical to overcome the continual build-up of residual strain ( $\varepsilon_p$ ) during cyclic actuation to ensure consistent performance over the component's service life. The results from the 200-cycle actuation test are shown in figure 7. The  $\varepsilon_p$  in the laser-processed actuator caused by cyclic degradation was found to stabilize after approximately 150 cycles. Similar results have previously been presented in the literature where cyclic degradation accumulated during each loading cycle will stabilize between 100 and 200 cycles [27–29]. This stabilization is the result of the reorientation/stabilization of preferred martensite variants and development of dislocations during early cycles. Different thermomechanical treatments have been found to affect how quickly this stabilization process occurs as discussed by Sofla *et al* [28]. More notably, the  $\varepsilon_r$  remains almost unchanged after 200 cycles where only a 0.6% decrease was measured from the first and last cycle. Therefore, the low cycle performance of the laser-processed linear actuator was comparable to traditional SMA actuators.

## 4. Conclusions

In this work a state-of-the-art laser processing technology was demonstrated to improve the functionality of a NiTi wire linear actuator. The addition of a second memory allowed for two distinct actuations using controlled resistive heating. The performance of this novel linear actuator was characterized and a better understanding of the results has been obtained. The main findings were as follows:

- (1) Laser processing enabled the modification of thermomechanical properties in a monolithic NiTi SMA. Compared to the as-received material, the transformation temperatures were increased after laser processing allowing for the development of a two-memory linear actuator.
- (2) Dynamic actuation was achieved using resistive heating and the simplicity of the DC control method was demonstrated. Dynamic activation of SMAs via a passive control method (i.e. via ambient temperature) is now plausible.
- (3) Tensile tests identified significant differences in the stress–strain behaviour during the deformation of martensite in the as-received and laser-processed materials. Lüders-like deformation did not occur in the laser-processed material. Instead, strain-hardening took place during the reorientation of martensite. Also, the  $\sigma_M$  was found to be substantially higher for the laser-processed material due to higher phase transformation temperatures and the inherent temperature dependence of martensite stability.
- (4) The interaction between the two different regions of the linear actuator was identified during each stage of actuation. The substantially lower  $\sigma_M$  of the as-received material led to a much larger active strain in the as-received region. Following activation of the as-received region, the stress and temperature in the laser-processed region changed with increasing pre-strain, complicating the determination of total active strain.
- (5) From cyclic actuation testing  $\varepsilon_p$  was found to stabilize after approximately 150 cycles while  $\varepsilon_r$  remained almost constant over all 200 cycles.

## Acknowledgments

The authors would like to acknowledge the support of the Natural Sciences and Engineering Research Council of Canada ([www.nserc.ca](http://www.nserc.ca)) and the Canada Research Chairs Program ([www.chairs-chaire.gc.ca](http://www.chairs-chaire.gc.ca)).

## References

- [1] Meier H, Czechowicz A and Langbein S 2010 Smart control systems for smart materials *Proc. Int. Conf. on Shape Memory and Superelastic Technologies (Pacific Grove California)* pp 224–5
- [2] Ma N, Song G and Lee H J 2004 Position control of shape memory alloy actuators with internal electrical resistance feedback using neural networks *Smart Mater. Struct.* **13** 777–83

- [3] Ikuta K, Tsukamoto M and Hirose S 1988 Shape memory alloy servo actuator system with electrical resistance feedback and application for active endoscope *Proc. IEEE Int. Conf. on Robotics and Automation* vol 1 (Piscataway, NJ) pp 427–30
- [4] Dutta S M, Ghorbel F H and Dabney J B 2005 Modeling and control of a shape memory alloy actuator *Proc. IEEE Int. Symp. on Intelligent Control (Limassol, Cyprus)* pp 1007–12
- [5] Khandelwal A and Buravalla V 2009 Models for shape memory alloy behavior: an overview of modeling approaches *Int. J. Struct. Changes Solids-Mech. Appl.* **1** 111–48
- [6] Ikuta K 1990 Micro/miniature shape memory alloy actuator *Proc. IEEE Int. Conf. on Robotics and Automation* vol 3 (Cincinnati, OH) pp 2156–61
- [7] Kuribayashi K 1991 Improvement of the response of an SMA actuator using a temperature sensor *Int. J. Robot. Res.* **10** 13–20
- [8] Pozzi M and Airoidi G 1999 The electrical transport properties of shape memory alloys *Mater. Sci. Eng. A* **273–275** 300–4
- [9] Airoidi G and Pozzi M 1999 The electrical transport properties of shape memory alloys under a stress state *J. Eng. Mater. Technol.* **121** 108–11
- [10] Khan M I and Zhou Y N 2010 Innovative Processing Technologies, assignee. Methods and Systems for Processing Materials, Including Shape Memory Materials *World Patent Application* WO/2011/014962
- [11] Khan M I 2010 Pulsed Nd:YAG laser processing of nitinol *PhD Thesis* University of Waterloo, Waterloo, ON, Canada
- [12] Pequegnat A, Vlasov M, Daly M, Zhou N and Khan M I 2011 Dynamic actuation of a multiple memory material processed nitinol linear actuator *Proc. ASME 2011 Conf. on Smart Materials, Adaptive Structures and Intelligent Systems (Phoenix, AZ)* p 4994
- [13] Daly M, Pequegnat A, Zhou N and Khan M I 2011 Fabrication of a novel monolithic NiTi based shape memory microgripper via multiple memory material processing *Proc. ASME 2011 Conf. on Smart Materials, Adaptive Structures and Intelligent Systems (Phoenix, AZ)* p 4903
- [14] Daly M, Pequegnat A, Zhou Y and Khan M I 2011 Fabrication of a novel laser-processed NiTi shape memory microgripper with enhanced thermomechanical functionality *J. Intell. Mater. Syst. Struct.*
- [15] Daly M, Pequegnat A, Zhou Y and Khan M I 2012 Enhanced thermomechanical functionality of a laser processed hybrid NiTi–NiTiCu shape memory alloy *Smart Mater. Struct.* **21** 045018
- [16] Khan M I and Zhou Y 2010 Effects of local phase conversion on the tensile loading of pulsed Nd:YAG laser processed nitinol *Mater. Sci. Eng. A* **527** 6235–8
- [17] Khan M I and Zhou Y 2010 A method to locally modify shape memory and pseudoelastic properties *Proc. Int. Conf. on Shape Memory and Superelastic Technologies (Pacific Grove California)* pp 202–3
- [18] Tang W 1997 Thermodynamic study of the low temperature phase B19' and the martensitic transformation in near-equiatomic Ti–Ni shape memory alloys *Metall. Mater. Trans. A* **28** 537–44
- [19] Miller D and Lagoudas D 2001 Influence of cold work and heat treatment on the shape memory effect and plastic strain development of NiTi *Mater. Sci. Eng. A* **308** 161–75
- [20] Tam B, Khan M I and Zhou Y 2011 Mechanical and functional properties of laser-welded Ti–55.8 Wt Pct Ni nitinol wires *Metall. Mater. Trans. A* **42** 2166–75
- [21] Murasawa G, Kitamura K, Yoneyama S, Miyazaki S, Miyata K, Nishioka A and Koda T 2009 Macroscopic stress–strain curve, local strain band behaviour and the texture of NiTi thin sheets *Smart Mater. Struct.* **18** 055003
- [22] Liu Y, Xie Z, Van Humbeeck J and Delaey L 1998 Asymmetry of stress–strain curves under tension and compression for NiTi shape memory alloys *Acta Mater.* **46** 4325–38
- [23] Liu Y, Van Humbeeck J, Stalmans R and Delaey L 1997 Some aspects of the properties of NiTi shape memory alloys *J. Alloys Compounds* **247** 115–21
- [24] Liu Y, Xie Z L, Van Humbeeck J and Delaey L 1999 Effect of texture orientation on the martensite deformation of NiTi shape memory alloy sheet *Acta Mater.* **47** 645–60
- [25] Miyazaki S, Otsuka K and Suzuki Y 1981 Transformation pseudoelasticity and deformation behaviour in a Ti–50.6 at.% Ni alloy *Scr. Metall.* **15** 287–92
- [26] Miyazaki S, Kimura S, Otsuka K and Suzuki Y 1984 The habit plane and transformation strains associated with the martensitic transformation in Ti–Ni single crystals *Scr. Metall.* **18** 883–8
- [27] Eggeler G, Hornbogen E, Yawny A, Heckmann A and Wagner M 2004 Structural and functional fatigue of shape memory alloys *Mater. Sci. Eng. A* **378** 24–33
- [28] Sofla A Y N, Elzey D M and Wadley H N G 2008 Cyclic degradation of antagonistic shape memory actuated structures *Smart Mater. Struct.* **17** 1–6
- [29] Grossmann C et al 2008 Processing and property assessment of NiTi and NiTiCu shape memory actuator springs *Mater. wiss. Werkst. tech.* **39** 499–510